Supplementary Information

The relevance of Cr defects and photoelectrochemical water oxidation activity of monoclinic $PbCrO_4$ films

Jiahe Li,[a] Gaili Ke,[a] Minji Yang,[b] Guoliang Lv,[a] Lanyi Cao,[a] Wenjun Li,[a] Tao Han,[a] Wenrong Wang,[a] Yong Zhou[c] and Huichao He[a]*

[a]College of Materials and New Energy, Chongqing University of Science and Technology. Chongqing 401331, China.

[b]Synthetic Lubricant Oil and Grease Branch, Sinopec Lubricant *Co.*, *Ltd.*, Chongqing, 400039, China.

[c]Ecomaterials and Renewable Energy Research Center, School of Physics, University Nanjing, Nanjing 211102, China

*Corresponding Author

Email: hehuichao@cqust.edu.cn

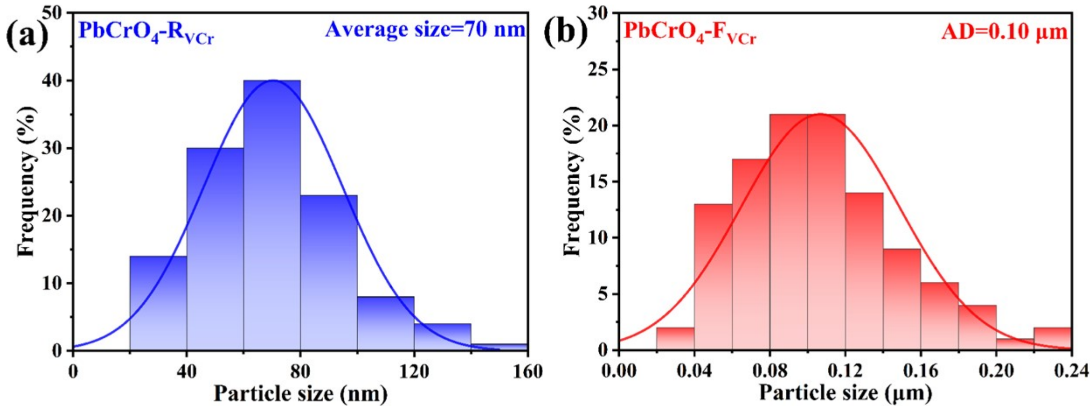

Fig. S1 The nanoparticles' size distribution of (a) $PbCrO_4$-R_{VCr} and (b) $PbCrO_4$-F_{VCr} films.

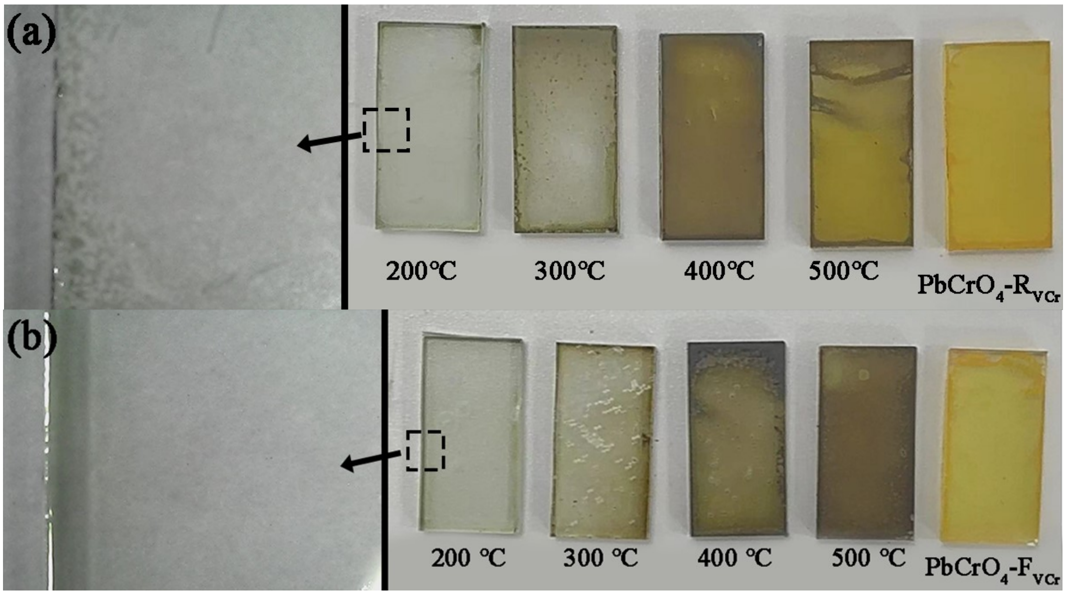

Fig. S2 The photographs of the Pb^{2+}/Cr^{3+} precursor solution during thermal treating at different temperatures for the preparation of (a) $PbCrO_4$-R_{VCr} and (b) $PbCrO_4$-F_{VCr} films.

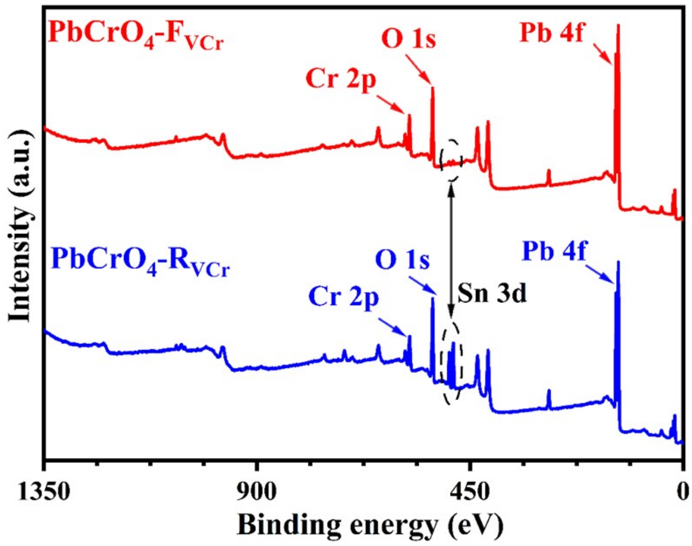

Fig. S3 Survey XPS spectrum of $PbCrO_4$-R_{VCr} and $PbCrO_4$-F_{VCr} films.

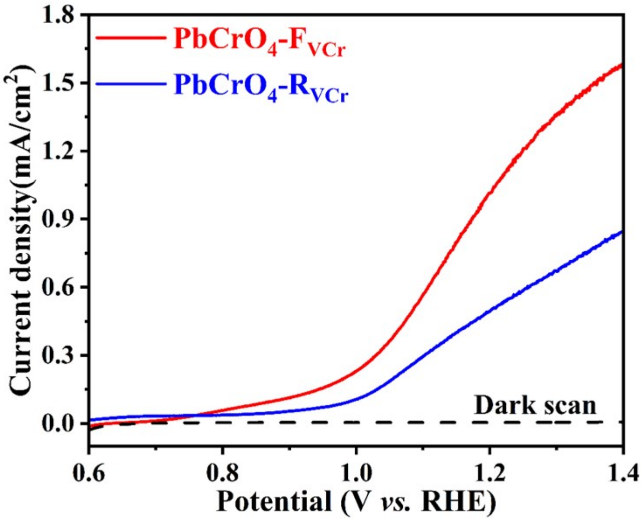

Fig. S4 Under AM 1.5G illumination, LSV curves of PbCrO$_4$-R$_{VCr}$ and PbCrO$_4$-F$_{VCr}$ film photoanodes in 0.5 M PBS.

Table S1 The activity comparison of our $PbCrO_4$-F_{VCr} film photoanodes to previously reported $PbCrO_4$ film photoanodes.

Electrolyte (pH)	J (mA/cm^2)	*Ref.*
0.5 M phosphate buffer (pH 7)	1.14 (at 1.23V *vs.* RHE)	**this work**
0.1 M Na_2SO_4 and 0.1 M Na_2SO_3(pH 7)	0.03 (at 0.4 V *vs.* Ag/AgCl)	[1]
0.1 M phosphate buffer (pH 6.8)	0.30 (at 1.23V *vs.* RHE)	[2]
0.1 M borate buffer (pH 9)	~0.10 (at 1.23V *vs.* RHE)	[3]
0.2 M phosphate buffer (pH 7)	0.57 (at 1.23V *vs.* RHE)	[4]
0.5 M phosphate buffer (pH 7)	2.70 (at 1.23V *vs.* RHE)	[5]
0.1 M phosphate buffer (pH 7)	0.06 (at 0.95V *vs.* RHE)	[6]
0.5 M phosphate buffer (pH 7)	3.43 (at 1.23V *vs.* RHE)	[7]
0.5 M phosphate buffer (pH 7)	~0.55 (at 1.23V *vs.* RHE)	[8]

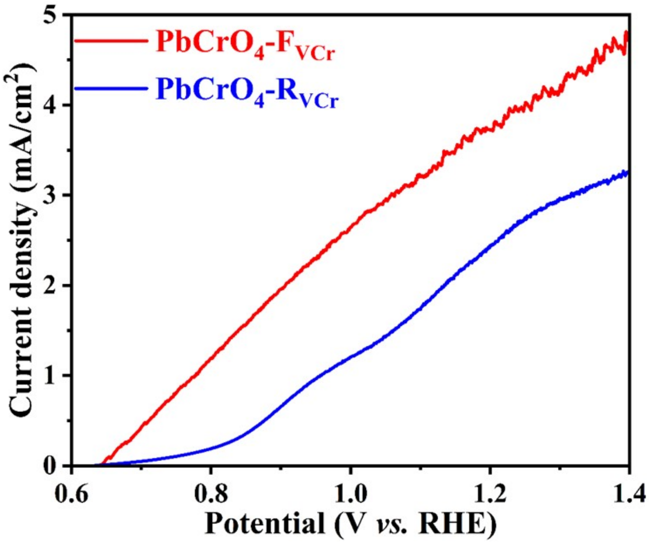

Fig. S5 Under AM 1.5G illumination, LSV curves of $PbCrO_4$-R_{VCr} and $PbCrO_4$-F_{VCr} film photoanodes in 0.5 M PBS/0.2 *vol.*% H_2O_2.

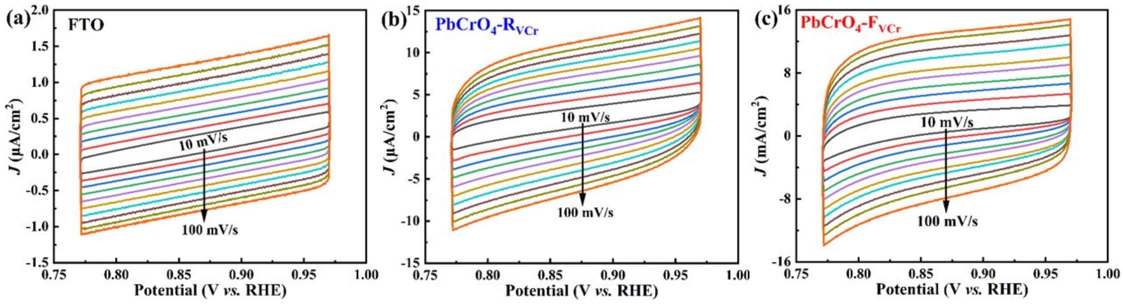

Fig. S6 CV curves of (a) FTO, (b) $PbCrO_4$-R_{VCr}, (c) $PbCrO_4$-F_{VCr} at different scan rates (10, 20, 30, 40, 50, 60, 70, 80, 90 and 100 mV/s).

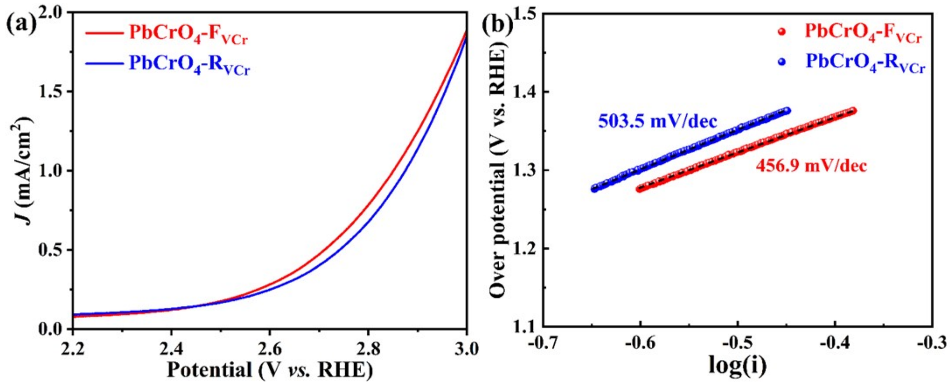

Fig. S7 In dark condition, (a) LSV curves and (b) Tafel plots for $PbCrO_4$-R_{VCr} and $PbCrO_4$-F_{VCr} film electrodes in 0.5 M PBS.

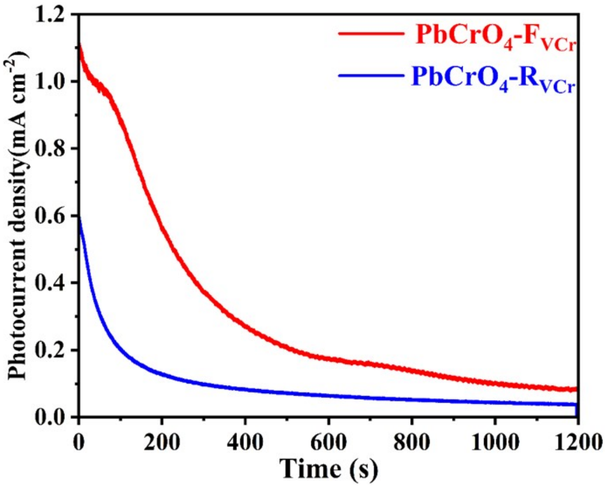

Fig. S8 *j*-t curves of $PbCrO_4$-R_{VCr} and $PbCrO_4$-F_{VCr} film photoanodes in 0.5 M PBS under AM 1.5 G irradiation at 1.23 V *vs*. RHE.

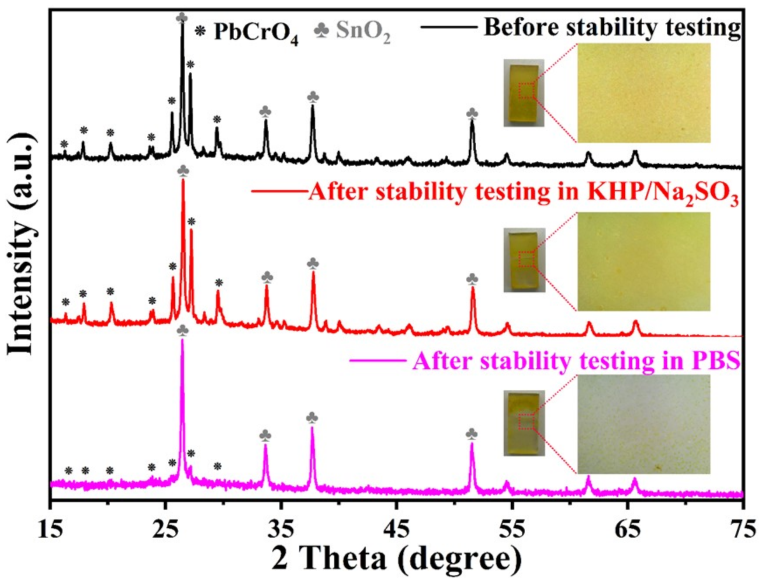

Fig. S9 XRD patterns of $PbCrO_4$-F_{VCr} films before and after stability testing in KHP/Na_2SO_3 (shown in **Fig. 5d)** and PBS (shown in **Fig. S8)** electrolyte.

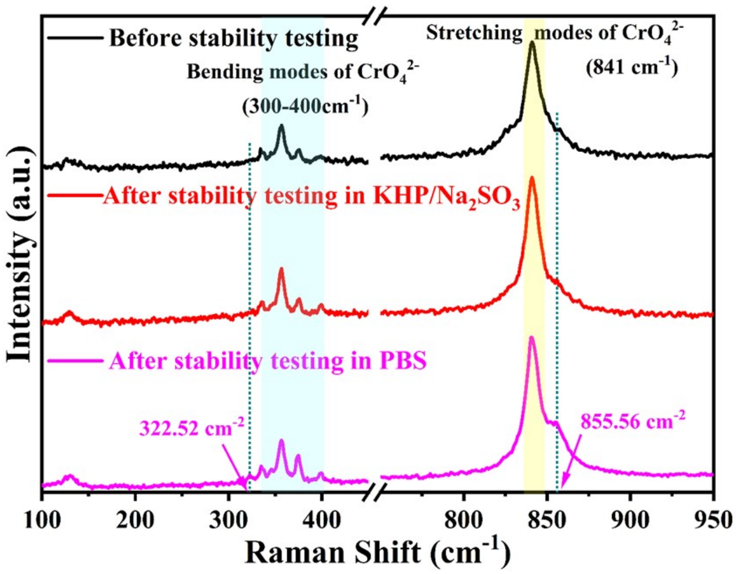

Fig. S10 Raman spectra of $PbCrO_4$-F_{VCr} films before and after stability testing in KHP/Na_2SO_3 (shown in **Fig. 5d)** and PBS (shown in **Fig. S8)** electrolyte.

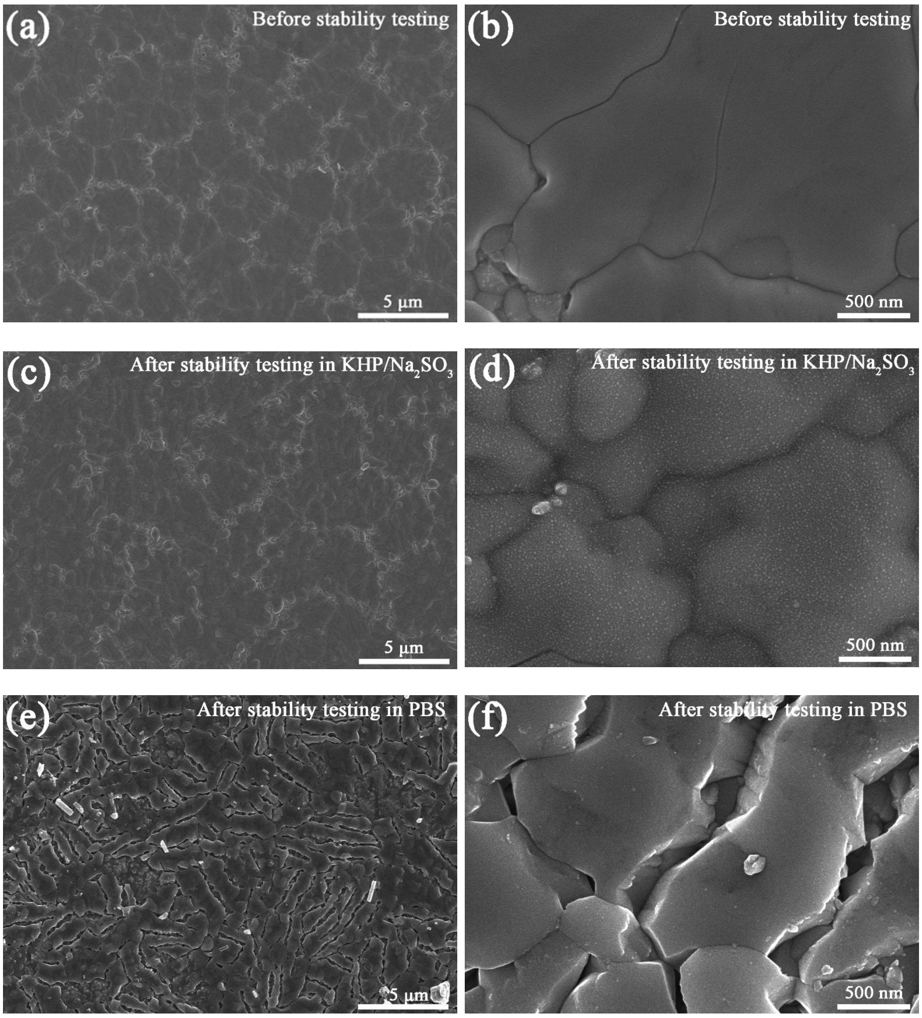

Fig. S11 SEM images of $PbCrO_4$-F_{VCr} films (a, b) before and after stability testing in (c, d) KHP/Na_2SO_3 (shown in **Fig. 5d)** and (e, f) PBS (shown in **Fig. S8)** electrolyte.

Table S2 The simulated ion activity product (IAP) and saturation index (*Sat.* index) of $PbCrO_4$ film in PBS solution.

Compound	*log IAP*	*Sat.* index	Saturation
$CrO_3(s)$	-22.232	-19.022	Undersaturation
$Pb_5(PO_4)_3(OH)$	-61.949	0.841	Oversaturation
PbO (Massicot)	2.14	-10.55	Undersaturation
PbO (Litharge)	2.14	-10.75	Undersaturation
$Pb(OH)_2(s)$	2.077	-6.073	Undersaturation
$Pb_2O(OH)_2(s)$	4.217	-21.973	Undersaturation
$Pb_3(PO_4)_2(s)$	-41.991	1.539	Oversaturation
$PbCrO_4(s)$	-20.092	-7.492	Undersaturation
$PbHPO_4(s)$	-22.097	1.708	Oversaturation
$PbO{:}0.3H_2O(s)$	2.119	-10.861	Undersaturation

Results and discussion for Fig. S9 to S11, and Table S2.

To understand the PEC stability feature of $PbCrO_4$-F_{VCr} films, we have detected the XRD patterns, Raman spectrum and SEM images for the $PbCrO_4$-F_{VCr} films after stability testing in KHP/Na_2SO_3 (shown in **Fig. 5d**) and PBS (shown in **Fig. S8**) electrolyte, respectively. As shown in **Fig. S9**, the XRD patterns of $PbCrO_4$-F_{VCr} film after stability testing in KHP/Na_2SO_3 are very close to those of it before stability testing. Meanwhile, the $PbCrO_4$-F_{VCr} film after stability testing in KHP/Na_2SO_3 had no obvious color change, relative to it before stability testing (insert of **Fig. S9**). But for the $PbCrO_4$-F_{VCr} film after stability testing in PBS, its XRD patterns partially changed, the diffraction peaks of monoclinic $PbCrO_4$ (PDF#: 08-0209) at 25.58^o, 27.16^o and 29.45^o disappeared. In addition, the color of $PbCrO_4$-F_{VCr} film after stability testing in PBS was turned to faint yellow, suggesting the presence of composition changes. Further Raman spectrum detections indicated that two new peaks (322.52 cm^{-1} and 855.56 cm^{-1}) be formed in the Raman spectrum of the $PbCrO_4$-F_{VCr} film after stability testing in PBS, compared with it before testing and testing in KHP/Na_2SO_3 (**Fig. S10**). SEM observations showed that the $PbCrO_4$-F_{VCr} film after stability testing in KHP/Na_2SO_3 has no obvious change in morphology (**Fig. S11c** and **S11d**), in comparison with it before testing (**Fig. S11a** and **S11b**). But after the stability testing in PBS, significant gaps were observed on the $PbCrO_4$-F_{VCr} film (**Fig. S113e** and **S11f**), indicating dissolution characteristics.

To understand the morphology change of $PbCrO_4$-F_{VCr} film photoanodes after stability testing in PBS, the ion activity product (*IAP*) and saturation index of compounds that could be potentially formed through the dissolution and transformation of $PbCrO_4$ in PBS solution were simulated using Visual MINTEQ software. The saturation index of compounds (*Sat.* index=$log(IAP/K_{sp})$) in aqueous solution above 0 uausally means potential dissolution tendency. As shown in **Table S2,** the saturation index of $Pb_5(PO_4)_3(OH)$, $Pb_3(PO_4)_2(s)$ and $PbHPO_4(s)$ could be formed through the transformation of $PbCrO_4$ in PBS solution, and their *Sat.* index are below 0, having dissolution tendency. Additionally, the semiconductors with variable valence state elements are easy to suffer from photocorrosion, since the electrons/holes of semiconductors cannot be transferred and consumed by reactions quickly, the cumulative electrons/holes in/on semiconductors could initiate photocorrosion through reacting with the variable valence elements of semiconductors [9]. Pb has two common valence states of +2 and +4, while Cr has +6 and +3. For $PbCrO_4$, its Pb is +2 and Cr is +6. During the PEC reaction on $PbCrO_4$ photoelectrodes, the Pb(II) could be oxided into Pb(IV) by the electrons of $PbCrO_4$, while the Cr(VI) could be oxided into Cr(III) by the holes of $PbCrO_4$ [8]. From above results and analyses, it can be known that $PbCrO_4$-F_{VCr} film photoanodes encounter photocorrosion and dissolution issue in PBS during stability testing.

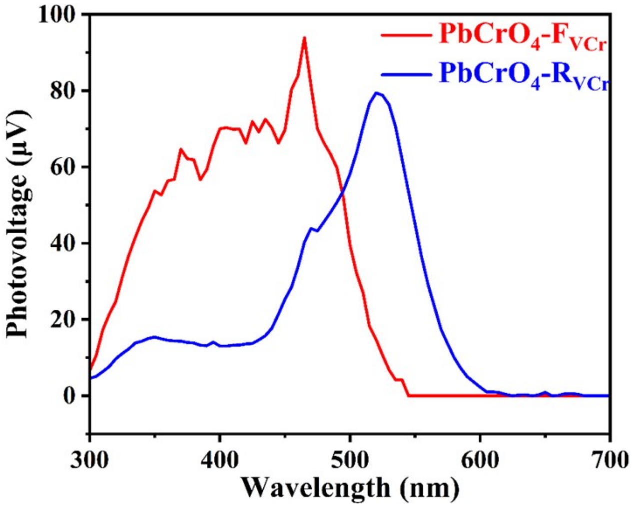

Fig. S12 Surface photovoltage spectra of $PbCrO_4$-R_{VCr} and $PbCrO_4$-F_{VCr} films in air.

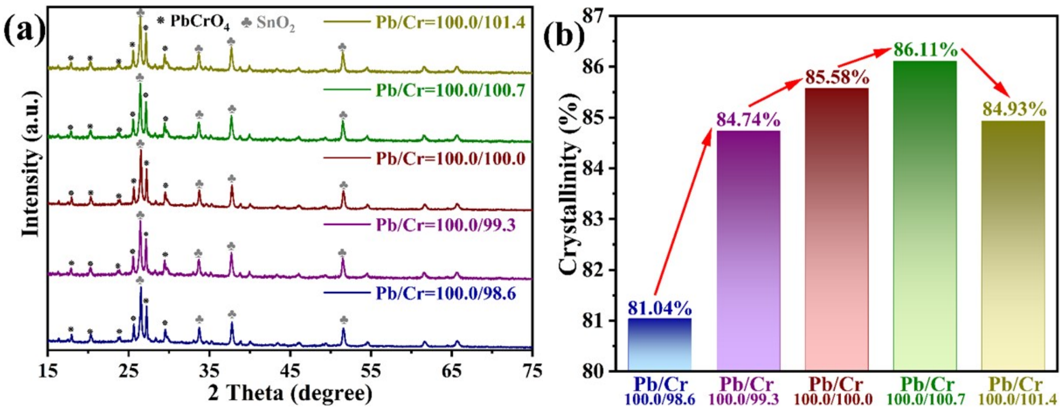

Fig. S13 (a) XRD pattern and (b) crystallinity of $PbCrO_4$ films which were prepared using precursor solution with different Pb/Cr atomic ratios.

Table S3 The crystallinities of $PbCrO_4$ films which were prepared using precursor solution with different Pb/Cr atomic ratios.

Sample	*hkl*	*2Θ*	*FWHM*	Crystallinity (%)
Pb/Cr=100.0/98.6	(200)	25.560	0.152	81.04
	(120)	27.149	0.120	
Pb/Cr=100.0/99.3	(200)	25.566	0.165	84.74
	(120)	27.150	0.148	
Pb/Cr=100.0/100.0	(200)	25.624	0.118	80.41
	(120)	27.218	0.107	
Pb/Cr=100.0/100.7	(200)	25.557	0.154	86.11
	(120)	27.143	0.138	
Pb/Cr=100.0/101.4	(200)	25.552	0.176	84.93
	(120)	27.146	0.146	

Reference

1. H. C. Lee, S. K. Cho, H. S. Park, K. M. Nam and A. J. Bard, *J. Phys. Chem. C*, 2017, **121**, 17561- 17568.
2. S. K. Cho, R. Akbar, J. Kang, W. Lee and H. S. Park, *J. Mater. Chem. A*, 2018, **6**, 13312- 13320.
3. A. E. Lindberg, W. Wang, S. Zhang, G. Galli and K. S. Choi, *ACS Appl. Energy Mater.*, 2020, **3**, 8658- 8666.
4. J. Kang, Y. R. Gwon and S. K. Cho, *J. Electroanal. Chem.*, 2020, **878**, 114601.
5. H. Zhou, D. Zhang, X. Gong, Z. Feng, M. Shi, Y. Liu, C. Zhang, P. Luan, P. Zhang, F. Fan, R. Li and C. Li, *Adv. Mater.*, 2022, **34**, 2110610.
6. W. Jiang, C. Ni, L. Zhang, M. Shi, J. Qu, H. Zhao, C. Zhao, R. Chen, X. Wang, C. Li, and R. Li, *Angew. Chem. Int. Ed.* 2022, **61**, e202207161.
7. H. Zhou, D. Zhang, H. Xie, Y. Liu, C. Meng, P. Zhang, F. Fan, R. Li and C. Li, *Adv. Mater.*, 2023, **35**, 2300914.
8. J. Li, Y. Huang, H. Wang, M. Yang, T. Han, G. Ke, W. Wang, H. Jiang and H. He, *Langmuir*, 2025, **41**, 20096–20104.
9. S. Chen, D. Huang, P. Xu, W. Xue, L. Lei, M. Cheng, R. Wang, X. Liu and R. Deng, *J. Mater. Chem. A*, 2020, **8**, 2286-2322.